Adv. Radio Sci., 6, 9–17, 2008
www.adv-radio-sci.net/6/9/2008/

Advances in Radio Science

Compact mode-matched excitation structures for radar distance measurements in overmoded circular waveguides

G. Armbrecht[1], E. Denicke[1], I. Rolfes[1], N. Pohl[2], T. Musch[3], and B. Schiek[3]

[1]Inst. für Hochfrequenztechnik und Funksysteme, Leibniz Universität Hannover, Appelstraße 9A, 30167 Hannover, Germany
[2]Lehrstuhl für Integrierte Systeme, Ruhr-Universität Bochum, Universitätsstraße 150, 44801 Bochum, Germany
[3]Institut für Hochfrequenztechnik, Ruhr-Universität Bochum, Universitätsstraße 150, 44801 Bochum, Germany

Abstract. This contribution deals with guided radar level measurements of liquid materials in large metal tubes, so-called stilling wells, bypass or still pipes. In the RF domain these tubes function as overmoded circular waveguides and mode-matched excitation structures like waveguide tapers are needed to avoid higher order waveguide modes. Especially for high-precision radar measurements the multimode propagation effects need to be minimized to achieve submillimeter accuracy. Therefore, a still pipe simulator is introduced with the purpose to fundamentally analyze the modal effects. Furthermore, a generalized design criterion is derived for the spurious mode suppression of compact circular waveguide transitions under the constraint of specified accuracy levels. According to the obtained results, a promising waveguide taper concept will finally be presented.

1 Introduction

Since the 1980s radar is one of the fastest-growing technologies in the process instrumentation industry (Parker, 2002), e.g. for tank level control. Due to its robustness, flexibility and the simultaneously falling market prices of microwave components, radar systems are advantageous in comparison to other level technologies such as differential pressure level, ultrasonic, capacitance, and displacer measurement systems (Kielb and Pulkrabek, 1999). Basically, there are two different techniques of radar setups which can be subdivided by the way the RF signal propagates: free-space radiating and guided wave setups. In free-space applications, state-of-the-art radar systems can be utilized not only for general process gauging, but also for calibratable high-precision level detection in an industrial environment (Weiss, 2001). Especially many commercial radar systems are based on frequency modulated continuous wave (FMCW) technologies (Brumbi, 1995). These systems provide an accuracy of the distance error within the submillimeter range (Musch, 2003). In the other case, the radar signal is guided along a transmission line probe. Coaxial probes are commonly used for exploiting the dispersion-free TEM waveguide mode for accurate level detection. Another upcoming important application for industrial radar systems is the application of permanently built-in still pipes, as depicted in Fig. 1, consisting of metal tubes that are large with respect to the radar wavelength. The usage of such configurations can be superior compared to the free-space case, due to the well-defined conditions of the waveguide suppressing parasitic reflections of tank internals. Even level turbulences that are caused by stirrers, resulting in measurement inaccuracies by waves and foam, can be neglected.

If the level detection in still pipes is conducted by using the same antennas as in the free-space radiating system, the accuracy of the measurements is significantly deteriorated compared to the free-space application (Pohl and Gerding, 2007). In contrast to Sai and Kastelein (2006), for our purpose solely conventional detection and signal processing algorithms are applied due to the limited processing power and power consumption in standardized industrial environment, e.g. the popular HART protocol (Brumbi, 2000). The still pipe functions as an overmoded circular hollow metallic waveguide. The deterioration is caused by intermodal dispersion due to the appearance of higher order multimode propagation and additionally due to chromatic waveguide dispersion of every single mode itself. The observed effects are strongly related to the behavior of multimode fiber optical transmission lines. Hence, this contribution investigates novel taper approaches and design criterions for a broadband mode-matched transition between waveguides with different diameters of the cross section, that can be utilized as feeding sections for still pipes (see Fig. 1). The structures are

Correspondence to: G. Armbrecht
(armbrecht@hft.uni-hannover.de)

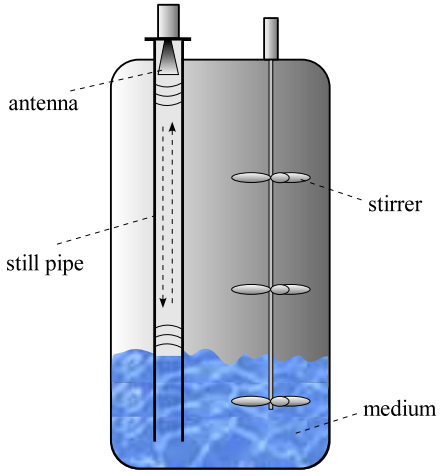

Fig. 1. Tank configuration incorporating a still pipe for accurate level detection.

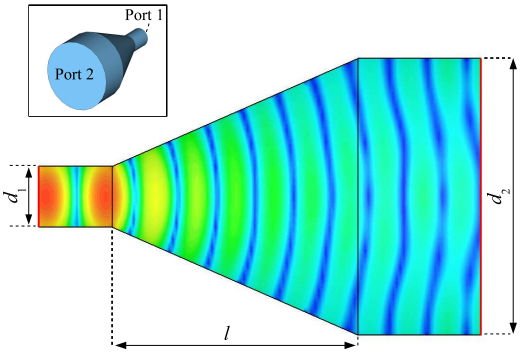

Fig. 2. Waveguide taper model of a two-port circular linear horn including the electric field at f=9.5 GHz (red color $\widehat{=}$max. amplitude) and typical geometrical settings.

optimized with respect to the conservation of the fundamental H_{11} field distribution between a single-moded small circular waveguide and an overmoded large circular waveguide by providing solely the excitation of the fundamental mode, i.e. the H_{11} mode, in an overmoded waveguide over a wide frequency range from 8.5 up to 10.5 GHz.

Characteristic optimization values are either the modal transmission coefficients, given in terms of scattering parameters of a two-port model derived from a commercial 3-D FIT field simulator, or the resulting FMCW distance error that is provided by a still pipe simulator incorporating all the modal and dispersive effects inside a still pipe. Realistic applications limit the space requirements of such transition geometries which results in a high demand for compact mode-matched structures. Thus, the maximal geometrical dimensions are limited. The lengthwise extension as well as the diameter at the second port are set to a value of l=d_2=80 mm to realize a transition starting from a feeding waveguide incorporating a fixed diameter of d_1=22 mm.

In the following, the structure of this article will be given: in Sect. 2 the general properties of a prominent waveguide taper will be introduced. Section 3 deals with the complete radar system and its simulation by utilizing a MATLAB implemented still pipe simulator, incorporating the mentioned dispersion and distortion effects. Subsequently, an analytical model of a waveguide transition is used for an in-depth analysis of the intermodal dispersion effects, providing the fundamentals for the derivation of an adequate design criterion in Sect. 3.3 that is directly related to the obtained measurement deterioration. Finally, according to this criterion, in Sect. 4 a novel subreflector-based taper concept will be shown.

2 Compact waveguide tapers

The simplest way to realize a compact waveguide transition is to use a conical horn with circular cross-section, as depicted in Fig. 2. Such a linear horn consists of a cone structure and is excited at the apex of the cone at a small diameter d_1. The impinging fundamental H_{11} field distribution, which exhibits planar phase fronts at the small cross section, is transformed into the corresponding spherical eigenmode inside the cone (Narasimhan and Balasubramanya, 1974). The H_{11} field distribution is mapped to spherical phases fronts with marginal higher order mode excitation within the cone itself. In general, the longer the horn structure the more the curvature of the phase fronts decreases. For the limit of an infinitely long cone, the fundamental H_{11} mode distribution will be completely conserved, when passing into a cylindrical eigenmode system at port 2 (see also Table 1).

In accordance with Fig. 2, a circular horn of *finite* length acting as a transition between cylindrical circular waveguides with different diameters is considered. A multiplicity of modes will be excited, due to the spherical phase fronts in the large waveguide. This kind of multimode excitation is primarily caused by the geometrical discontinuity at the transition to the large circular waveguide, due to the change in the corresponding eigenmode system. Even if discontinuities are similar to those at the feeding section (port 1), the influence on the mode conversion behavior of the taper is much smaller. All of the higher order modes are below their cut-off frequencies f_c. Figure 3 shows the scattering parameters S_{21} for the proposed circular linear horn in the frequency range from 8.5 up to 10.5 GHz, where $\left|S_{2(\text{Mode x}),1(\text{H}_{11})}\right|$ denotes the magnitude of the mode conversion between the fundamental mode at port 1 and multimode excitation at port 2.

Theoretically, a total number of 41 cylindrical modes are able to propagate in such a still pipe at the large diameter d_2. However, not all of these modes have to be taken into account for the taper investigation. According to Tang (1966), in case of distinct polarization properties of the incident H_{11} mode

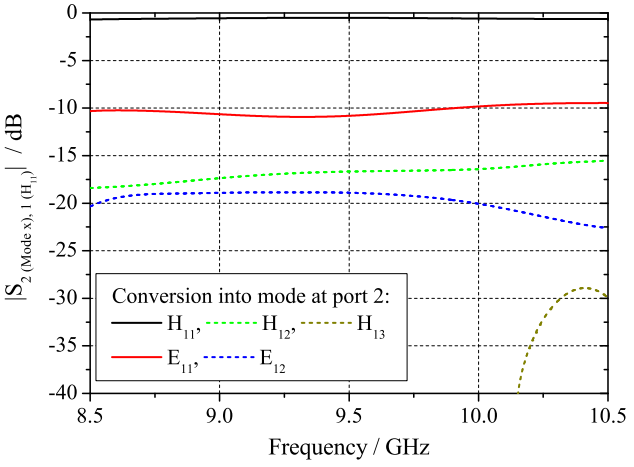

Fig. 3. Mode conversion from the fundamental mode H_{11} at port 1 into a mixture of different modes at port 2.

and under the assumption of axial straight and radial symmetrical waveguide tapers, the total number of modes with noticeable excitation reduces significantly to five. Solely H_{1p} and E_{1p} modes are excitable, if the respective cut-off frequencies f_c are passed. As shown in Fig. 3, the first higher order mode E_{11} is constantly suppressed by approximately 10 dB over the whole frequency range of interest. The other eigenmodes are more attenuated, so E_{11} is identified as the dominant higher order mode. The results given in Fig. 3 are representative for any kind of waveguide taper that is to be considered in this paper, regardless of the exact shape or filling. Hence, in the following sections the E_{11} mode is anticipated to have the major effects on potential intermodal dispersion inside a still pipe. If the total horn length would be a degree of freedom, Table 1 denotes the distinct improvements in the derived mode conversion behavior depending solely on length extension, showing the steady reduction of the parasitic eigenmodes at the center frequency of f=9.5 GHz. This trivial solution is well-known and will therefore not be considered in our evaluation.

3 Still pipe simulation

In this section the features and the underlying analytical formulations of a MATLAB implemented still pipe simulator are introduced, yielding the possibility to verify the waveguide tapers directly by means of the overall gauging performance. The accuracy prediction is an important figure of merit, especially for the design and optimization process of novel taper structures. Thus, an existing measurement setup is emulated in software by utilizing analytical waveguide equations to account for the loss-free mode-dependent wave propagation behavior inside the metal pipe (Barrow, 1984). The setup is schematically depicted in Fig. 4. The setup approximates the expected reflections caused by arbitrary material properties of liquids in terms of a movable plane sliding short within the still pipe. Thus, modal coupling and conversion at this reflector can be neglected (Katsenelenbaum and Mercader, 1998) and the reflection coefficients for all $N-1$ eigenmodes are equally set to $\Gamma_n=-1$ (cp. Eq. 3). Without loss of generality it is advantageous to choose magnitudes of $|\Gamma_n|<1$ to attenuate the radar signal. Therefore, multiple signal reflections and resulting ringing can be reduced that could cause aliasing effects due to undersampling by exceeding the range of unambiguity. Generally, the range of unambiguity is determined by the number of frequency samples N_s, whereas N_s=1001 samples over a total bandwidth of Δf=2 GHz were evaluated. Signal interpolation in time domain can be considered via zeropadding in the frequency domain.

Table 1. Magnitudes of the conversion of the H_{11} mode into the spurious cylindrical waveguide modes E_{11}, H_{12}, E_{12} and H_{13} in dependence of the total linear horn length at the center frequency of f=9.5 GHz.

l / mm	80	160	240	320
$S_{2(E_{11}),1(H_{11})}$/dB	−10.8	−15.5	−19.5	−21.1
$S_{2(H_{12}),1(H_{11})}$/dB	−16.7	−22.6	−25.8	−28.2
$S_{2(E_{12}),1(H_{11})}$/dB	−18.9	−27.9	−33.8	−31.2
$S_{2(H_{13}),1(H_{11})}$/dB		below f_c		

According to Fig. 4 the whole system configuration consists of the excitation structure and the still pipe, whereas the reflection coefficient Γ_{res} represents the transfer function of the complete radar setup. FMCW measurements can be simulated by solely evaluating the real part of the reflection coefficient which results in an image error, as shown by Stolle and Heuermann (1995). Additionally, various window functions can be applied. For our investigations the Hannning window W_{Hann} is used. Subsequently, an inverse Fourier transform provides the impulse response, whereas solely the envelope is evaluated. Common signal processing algorithms, e.g. barycentric pulse detection (Le Huerou and Gindre, 2003), can be utilized, even though the still pipe is a dispersive transmission line. Minimal deteriorations are obtained, if the still pipe is used in single-mode operation considerably beyond the cut-off frequency $f_{c,\mathrm{H}_{11}}$ of the desired H_{11} mode. The determined pulse round trip time is then converted into the particular measurement distance by multiplying with the broadband average signal velocity $\overline{v}_{\mathrm{gr,H}_{11}}$, as given by Eq. (1). This equation accounts in an appropriate manner for the frequency-dependent and mode-specific propagation properties.

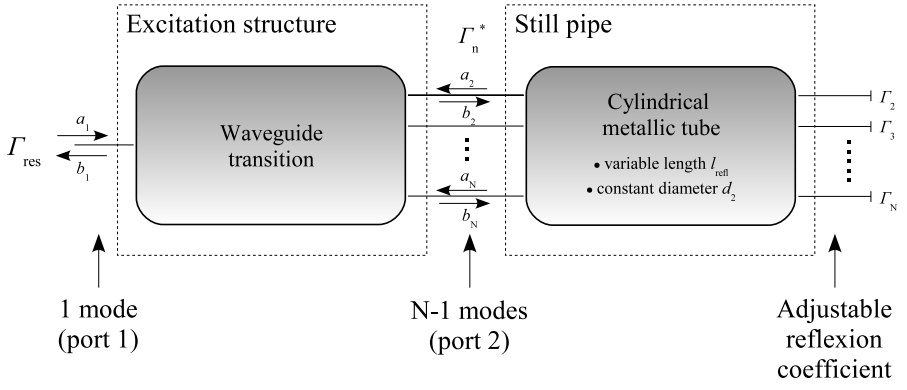

Fig. 4. Scheme of the MATLAB-based still pipe simulation.

$$\overline{v}_{\mathrm{gr,H_{11}}} = \frac{\sum_{k=1}^{N_s} \left(|S_{21}(f_k)| \cdot W_{\mathrm{Hann}}(f_k)\right)^2 \cdot v_{\mathrm{gr,H_{11}}}(f_k)}{\sum_{k=1}^{N_s} \left(|S_{21}(f_k)| \cdot W_{\mathrm{Hann}}(f_k)\right)^2} \quad (1)$$

$$\text{with} \quad v_{\mathrm{gr,H_{11}}}(f_k) = \frac{1}{\sqrt{\varepsilon\mu}} \sqrt{1 - \left(\frac{f_{c,\mathrm{H_{11}}}}{f_k}\right)^2}$$

Equation (1) derives from summing up all monofrequent group velocities $v_{\mathrm{gr,H_{11}}}(f_k)$, each weighted with its individual spectral power, normalizing the entire sum to the total signal power. N_s specifies the frequency samples, whereas $|S_{21}(f_k)|$ denotes the magnitude of conversion into the desired $\mathrm{H_{11}}$ mode. ε and μ stand for the material permittivity and permeability, respectively. The formulation is derived in accordance to a similar pulse delay equation given by Hartog (1979). The excitation structure is described as a physical two-port device exhibiting N virtual port modes, one at the first and $N-1$ eigenmodes at the second port. Therefore, the whole waveguide transition can fully be described by a $N \times N$ scattering matrix, as follows:

$$\begin{pmatrix} b_1 \\ \vdots \\ b_N \end{pmatrix} = \begin{bmatrix} S_{11} & \cdots & S_{1N} \\ \vdots & \ddots & \vdots \\ S_{N1} & \cdots & S_{NN} \end{bmatrix} \cdot \begin{pmatrix} a_1 \\ \vdots \\ a_N \end{pmatrix}. \quad (2)$$

In Eq. (2) a_n and b_n denote the nth incident and reflected wave quantities, respectively. Whereas the reflected waves b_n at the second port can be expressed by the transformed reflection coefficient Γ_n^* of the still pipe, as given by Eq. (3).

$$b_n = \Gamma_n^* \cdot a_n = \frac{1}{\Gamma_n} \cdot e^{2\gamma_n l_{\mathrm{refl}}} \cdot a_n \quad \forall \quad n \geq 2 \quad (3)$$

The parameter γ_n stands for the wave propagation constant of the nth cylindrical waveguide mode. Thus, the reflected wave quantities in Eq. (2) are consequentially substituted according to Eq. (3), leading to a reduction to the wave quantity b_1, as follows:

$$\begin{pmatrix} b_1 \\ 0 \\ \vdots \\ 0 \end{pmatrix} = \overbrace{\begin{bmatrix} S_{11} & S_{12} & \cdots & S_{1N} \\ S_{21} & S_{22} - \Gamma_2^* & \cdots & \vdots \\ \vdots & \vdots & \ddots & \vdots \\ S_{N1} & \cdots & \cdots & S_{NN} - \Gamma_N^* \end{bmatrix}}^{[S_{\mathrm{mod}}]} \cdot \begin{pmatrix} a_1 \\ a_2 \\ \vdots \\ a_N \end{pmatrix}. \quad (4)$$

S_{mod} denotes the modified scattering matrix exhibiting solely one single output coefficient b_1 and combining the unknown incident waves in terms of the vector quantity $\boldsymbol{a}$. The set of linear equations is solved by setting the value of b_1=1 and inverting the derived matrix $[S_{\mathrm{mod}}]$.

$$\boldsymbol{a} = [S_{\mathrm{mod}}]^{-1} \cdot (1, 0 \cdots 0)^{\mathrm{T}}, \quad (5)$$

Subsequently, Γ_{res} is given by:

$$\Gamma_{\mathrm{res}} = \frac{b_1}{a_1} = a_1^{-1}, \quad (6)$$

concerning all system components including the full-wave simulation results of the mode conversion behavior of arbitrary waveguide transitions. Hence, on the basis of the still pipe simulator, fundamental evaluation of the intermodal and chromatic dispersion can efficiently be performed. In the following sections, insights to the design constraints will be given with respect to the mode conversion properties of a waveguide transition. As already shown in Sect. 2, due to geometry, polarization and symmetry properties of the regarded cylindrical waveguide transitions, the maximal degree of the mode index is set to N=6 for further investigations.

3.1 Analytical model of a waveguide transition

An analytical model of a waveguide transition will be presented leading to a direct relationship between the level of

spurious mode excitation at port 2 and the measurement uncertainties and thus providing the fundament of modal design rules for still pipe excitation structures. The choice of modal level can be adjusted by determinating the modal transmission parameters S_{n1} into each mode (with $2 \leq n \leq N$). These scattering parameters are assumed to have purely real values, i.e. the phase is neglected and therefore the spatial extension is set to zero.

Considering loss free, isotropic and passive waveguide structures, the corresponding scattering matrix will become reciprocal (cp. Eq. 7) and unitary (cp. Eq. 9). The complete scattering matrix accounts for the matching properties of such a N-port structure, thus being comparable with a three-port device that cannot be matched at all ports. In this case, the multimode waveguide transition cannot be matched for every single mode, which arises mode-dependent multiple reflection cycles inside the tube. A serious consequence are pulse replica within the system's impulse response, which may exceed the peak amplitudes of the first pulse. This originates from a phenomenon similar to the mode beating effect well-known from the theory of optical transmission line (Fernandez Casares and Balle, 1994). As a result, the applied barycentric processing algorithm unlatches due to the inaccurate pulse maximum detection on pulse replica.

Exemplary, $N=3$ is considered for the following evaluation, resulting in solely one parasitic mode, i.e. the incident mode power is purely split up in the modes H_{11} and E_{11}, respectively. By incorporating the principal of reciprocity, given by:

$$[S] = [S]^{\mathrm{T}}, \tag{7}$$

the corresponding scattering matrix is given by Eq. (8), whereas the assumption $S_{11}=0$ is chosen to approximate a perfect matched excitation port, as follows:

$$[S_{\mathrm{ana}}] = \begin{bmatrix} 0 & S_{21} & S_{31} \\ S_{21} & \boldsymbol{S_{22}} & \boldsymbol{S_{23}} \\ S_{31} & \boldsymbol{S_{23}} & \boldsymbol{S_{33}} \end{bmatrix}. \tag{8}$$

Thus, the three unknown quantities are the marked scattering parameters S_{22}, S_{33} and S_{23}. Hence, utilizing the assumed unitarity, a set of nonlinear equations is derived from the equations

$$[S]^{\mathrm{T}}\,[S]^{*} = [S]^{*\mathrm{T}}\,[S] = [I] \quad \Leftrightarrow \quad [S]^{-1} = [S]^{*\mathrm{T}} \tag{9}$$

and is subsequently solved numerically. In Eq. (9), $[I]$ denotes the identity matrix, $(^*)$ accounts for the complex conjugate operation and $(^{\mathrm{T}})$ stands for the transpose of matrix. The phase of the unknown three parameters reaches merely two discrete values of 0° and 180°, due to absent spatial extension. In general, solving the nonlinear system numerically for $N>3$ becomes more complex, because it is overdetermined, however, also includes redundancies among the equations itself. This causes ambiguities in the solution strongly depending on the choice of the initial values for the unknowns. The total number of unknowns is given by $(N^2-N)/2$.

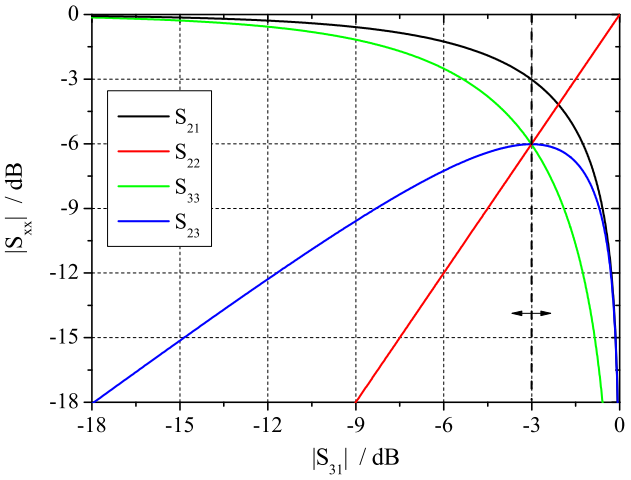

Fig. 5. Scattering parameters for a virtual 3×3 transition in dependence of the parasitic transmission level of $|S_{31}|$.

Finally, the derived analytical waveguide transition can be utilized for the generation of scattering matrices having user-defined spurious modal transmission levels, as depicted in Fig. 5 for the special case of $N=3$. Here, the parameter S_{31} accounts for the excitation of the parasitic mode E_{11} that entirely defines the remaining parameters, e.g. for a mode level of $S_{31}=-3$ dB, S_{21} takes the same value whereas $|S_{22}|=|S_{33}|=|S_{23}|=-6$ dB is derived. Henceforth, the analytical waveguide transition is utilized to characterize intermodal dispersion effects in still pipes that refers to constant modal conversion levels over arbitrary frequency ranges.

3.2 Intermodal dispersion

This section focuses on the analysis of intermodal dispersion, which significantly determines the influences on the measurement uncertainties. Accurate detection properties are achieved when, due to temporal walk-off, pulse breakup has occurred (Shum, 2004), i.e. the individual modes' pulses have sufficiently separated. The chromatic dispersion is negligible causing rather small pulse distortion due to the low cut-off frequency of the H_{11} operational mode. In Fig. 6 the obtained impulse response for a distinct reflector position at $l_{\mathrm{refl}}=3$ m is depicted, accounting for two different reflection coefficients $|\Gamma_{\mathrm{n}}|=0.5 \vee 1$. The pulse package consists of the two superimposed modes, i.e. H_{11} and E_{11}, equally excited and thus splitted to -3 dB. The subdivision directly refers to Sect. 3.1 and the marked scattering parameters shown in Fig. 5. In both cases the signal energy incorporated by the pulse packages is more and more spread with increasing numbers of reflection, whereas the major difference is observed to be the signal-to-noise ratio (SNR). At $|\Gamma_{\mathrm{n}}|=1$ the

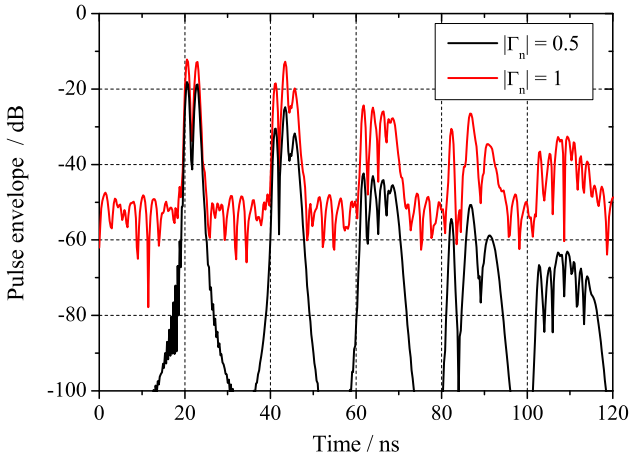

Fig. 6. Multiple reflections of the fundamental H_{11} and the first spurious E_{11} mode in dependence of the reflection coefficient $|\Gamma_n|$

SNR value is raised about 50 dB compared to the reflection coefficient of $|\Gamma_n|=0.5$. As already mentioned in Sect. 3, this is a result of signal ringing. To avoid the arising undersampling phenomenon, an appropriate value of $|\Gamma_n|$ is chosen for further investigations. For the investigation the total number of ports $N=4$ is considered, which specifies two parasitic modes (E_{11}, H_{12}). The adjustable reflector distance of the simulated still pipe is given in an interval of $l_{refl}=[0\ldots5\,\mathrm{m}]$, while the step width is chosen to $\Delta l_{refl}=l_{refl,max}/1000$. Subsequently, the graphs are scaled and normalized in terms of an equivalent non-dispersive pulse propagation without any attenuation, being fully reflected. When measuring with a FMCW radar technology, solely the real part of the derived total reflection coefficient Γ_{res} is evaluated; the peak pulse amplitude becomes bisected to -6 dB. Multimode propagation and thus arising mismatches at the transition site in combination with reflector losses will result in a decrease of the peak pulse amplitudes, if a fixed total incident power level is provided. For an in-depth investigation of the intermodal dispersion of the first pulse package, the same reflector distance $l_{refl}=3$ m is chosen in combination with a fixed total parasitic mode power of 25%, according to the incident mono-mode power at port 1. At this power level, pulse replica influences are not of any concern. Therefore, the explicit pulse shape deterioration by intermodal dispersion solely of the first incoming package is depicted in Fig. 7a for different mode configurations. The mono-mode H_{11} pulse is well-shaped without any observable indication of chromatic dispersion. In contrast to the curve including the spurious E_{11} mode, the obtained package consists of two pulses, whereas the E_{11} pulse is delayed due to its increased cut-off frequency. If E_{11} is exchanged by H_{12}, that exhibits an even higher cut-off frequency compared to E_{11}, the pulse delay as well as the H_{12} pulse spread is raised and thus leads to an improvement in intermodal pulse separation. Finally, the excitation of both spurious modes is equally combined resulting in attenuated pulses without influencing the absolute pulse position in time domain.

This leads to the assumption, that the excitation of merely the E_{11} mode represents the worst case scenario for the barycentric signal detection algorithm. This pulse package is affected by the longest displacement of the barycenter, that results in an increase in measurement uncertainties. In detail, the described behavior is depicted in Fig. 7b, showing the simulated distance error e over the entire reflector range from $l_{refl}=0$ up to 5 m. At the distinct position of $l_{refl}=3$ m, having been already evaluated, the obtained error for all sets of modes is negligible because a sufficient level of pulse separation is obtained. Generally, in the close-up range of $l_{refl}\leq0.2$ m the distance inaccuracies of all sets are similarly affected by the FMCW image error. Further errors caused by a finite input matching of the analytical waveguide transition are excluded, as given by Eq. (8). Therefore, this range is not considered for further investigations. According to Fig. 7b, all curves have an oscillating characteristic that is caused by the already mentioned pulse beating deterioration. As expected, considering the entire reflector interval l_{refl} the excitation of solely the E_{11} mode exhibits the longest influence on the error curve, followed by H_{12} causing the same peak error of approximately $e_{max}=20$ mm, however, decaying much faster with increasing reflector distances.

Finally, the combination of these two spurious modes results in a smaller peak error, due to the constant parasitic power level now is split into two modes, which is therefore advantageous for real taper design. If the influences of H_{12} have completely decayed starting from a distinct reflector position of $l_{refl}\approx1.2$ m, the E_{11} error characteristic remains, obtaining the same decaying length.

3.3 Design criterion for waveguide tapers

The aim of this section is to quantify the level of mode suppression that is necessary to achieve submillimeter accuracy. In accordance with the investigated intermodal dispersion behavior in the previous Sect. 3.2, the exclusive excitation of the E_{11} mode marks the worst case scenario to cope with. Therefore, in the present section a design criterion is derived, especially accounting for the first spurious mode. Based on experience with real waveguide taper, improvement in parasitic mode suppression is limited to a certain frequency range. Hence, the criterion is extracted by assuming a spurious E_{11} mode magnitude of $\left|S_{2(E_{11}),1(H_{11})}\right|=-20$ dB over a bandwidth ranging in an interval of $\Delta f_{notch}=[0\ldots2\,\mathrm{GHz}]$. Obviously, a certain amount of bandwidth of the proposed suppression level is required. Δf_{notch} is located around the center frequency of $f=9.5$ GHz, where the radar system is supposed to have highest sensitivity compared to the corner frequencies due to the applied signal processing window.

Therefore, an analytical waveguide taper ($N=3$) having a stepwise constant scattering parameter S_{31} accounting for

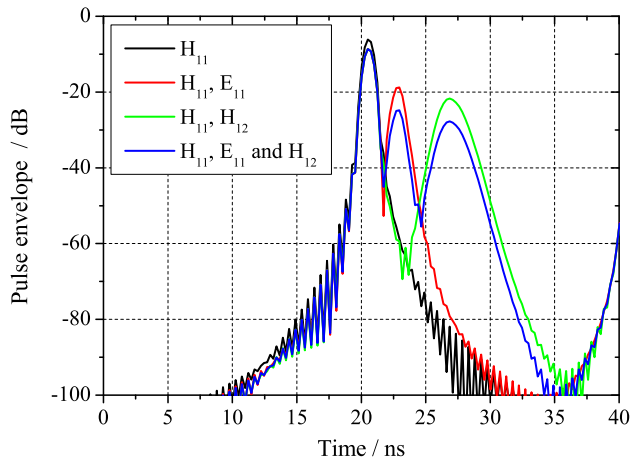

(a) Impulse responses at l_{refl}=3 m

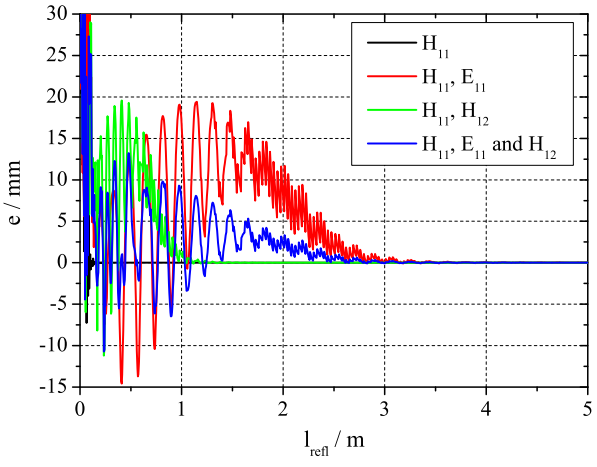

(b) Distance error e over the entire range

Fig. 7. Time signal and corresponding distance error for four sets of eigenmodes including H_{11}, E_{11} and H_{12}.

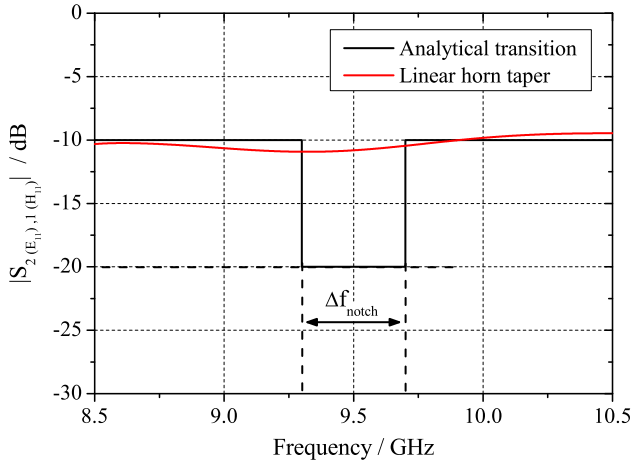

(a) Frequency dependent E_{11} mode suppression

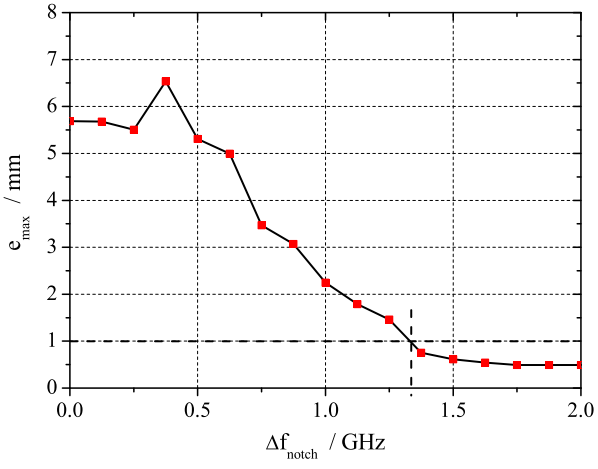

(b) Maximal distance error e_{max}

Fig. 8. Worst case estimation of the level of E_{11} mode suppression in dependence of the required bandwidth.

the transmission properties of $|S_{2(\mathrm{E}_{11}),1(\mathrm{H}_{11})}|$ is utilized, as introduced in Sect. 3.1. The corresponding characteristic is depicted in Fig. 8a starting from the approximation of the circular linear horn at a constant E_{11} magnitude of $|S_{2(\mathrm{E}_{11}),1(\mathrm{H}_{11})}| = -10$ dB, as shown in Sect. 2. In Fig. 3.2 the obtained maximal distance error e_{max} is shown depending on the value of $\Delta f_{\mathrm{notch}}$ for $0.2\,\mathrm{m} < l_{\mathrm{refl}} < 5\,\mathrm{m}$. As depicted, the error continuously decreases with rising values of the notch bandwidth $\Delta f_{\mathrm{notch}}$. At a distinct bandwidth of $\Delta f_{\mathrm{notch}} \approx 1.3$ GHz the corresponding maximal distance error e_{max} is falling below the desired value of $e_{\mathrm{max}} < 1$ mm. Beyond this certain bandwidth the remaining accuracy level keeps within the submillimeter range. In summary, a direct relationship between the spurious mode suppression level and the obtained FMCW radar distance error is accomplished. Henceforth, real waveguide transitions can solely be evaluated by its spurious mode transmission behavior. Thus, the verification of every single step in the design and optimization process of waveguide tapers in terms of distance errors can be omitted, leading primarily to a raise in the design speed of novel taper structures.

4 Mode-matched excitation structures

Based on the derived design criterion according the previous Sect. 3.3, improved real waveguide taper concepts are considered by utilizing a commercial 3-D FIT solver (CST MICROWAVE STUDIO, Vers. 2006B) for numerical evaluation. To briefly review the major consequences drawn by the analysis of Sect. 2, the fundamental mode excitation purity of a circular linear horn taper obviously suffers from spherical phase fronts inside the cone. That results in an increase of transmission into the major spurious mode E_{11},

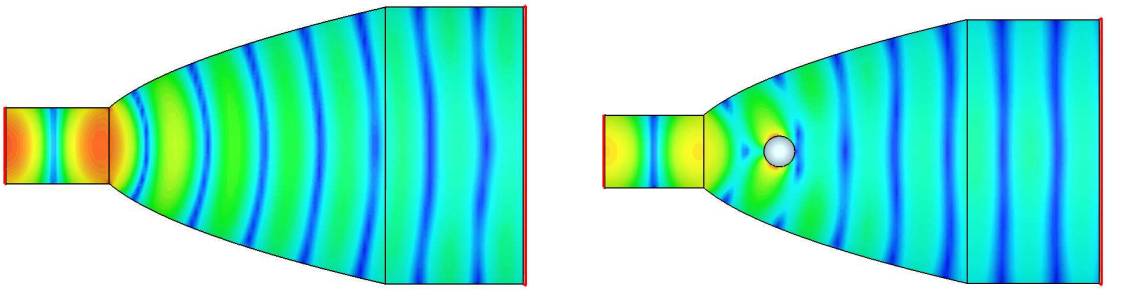

(a) Taper with paraboloidal shape **(b)**Taper with paraboloidal shape including a metallic sphere

Fig. 9. Electric field distribution at f=9.5 GHz in two different paraboloidal waveguide transitions.

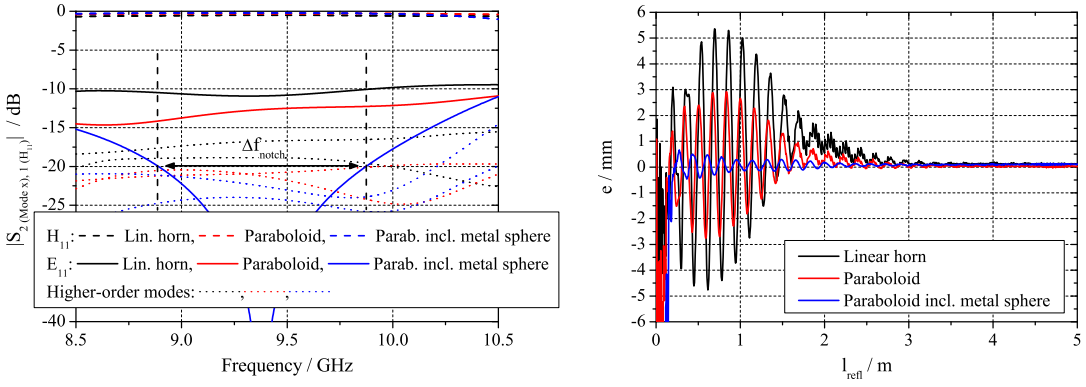

(a) Spurious mode suppression **(b)** Corresponding distance error e

Fig. 10. Comparison of three different waveguide tapers in terms of excited mode levels and obtained FMCW measurement uncertainties.

when changing back the eigenmode system from spherical to cylindrical at the second port. At first, well-known analogies from the ray-optics are considered, that may lead to a phase curvature reduction by solely changing the contour of the waveguide taper, so that the phase distribution becomes flattened. Whereas the distinct feature of straight phase fronts denotes for the possible evidence of a single-moded field distribution, it may not be considered as a general proof. Nevertheless, the phase characteristic can be utilized to support the design and optimization process. In the fictional case of a punctual isotropic radiating source in the focal point of a paraboloid, the reflected rays form a straight phase distribution in the plane of the second port. However, this analogy is purely valid when the rays, which are directly propagating in the direction of the second port, are neglected. Hence, our approach consists of a combination of both principles by exploiting the flattening effects of a taper exhibiting a parabolic shape and simultaneously suppressing the direct wave propagation through the whole taper structure by the insertion of an appropriate obstacle. The influence of the applied obstacle on the field distribution inside the taper structure is comparable to a subreflector of a Cassegrainian antenna feed system (Rusch, 1963). For our purpose to design mode-matched waveguide tapers, a metallic sphere was found to provide remarkable improvements.

Figure 9 depicts the achieved improvements regarding the phase distribution for two cases of parabolic transitions. According to the curvature of the phase fronts at the second port, the parabolic shape (see Fig. 9a) is advantageous compared to the distribution obtained by the circular linear horn, depicted in Fig. 2. Furthermore, when the metallic sphere is applied, an additional improvement can be observed. This behavior is verified by the simulated scattering parameter, as given in Fig. 10a. Subsequently, the mode magnitude level $\left|S_{2(\mathrm{E}_{11}),1(\mathrm{H}_{11})}\right|$ decreases, offering best results in case of the parabolic structure combined with the metallic obstacle. In this case, a notch bandwidth $\Delta f_{\mathrm{notch}} \approx 1.0$ GHz considering a E_{11} mode suppression level of more than 20 dB can be realized in the range of 8.9 GHz to 9.9 GHz. Other higher order modes are likewise suppressed by approximately more than 20 dB.

Figure 10b shows the derived distance error, in the same manner as introduced in Fig. 7b. The measurement uncertainties are successively decaying between the three structures, starting at a maximal error of about $e \approx 5$ mm in case of a linear horn, for the paraboloid taper a decreased maximal error of $e \approx 3$ mm is obtained. As expected, the best results are achieved by the paraboloid including the proposed metal sphere as a subreflecting obstacle, maintaining a continuous accuracy level of less than one millimeter. Although, the

notch bandwidth of this structure is less than the requested $\Delta f_{\text{notch}} \approx 1.3\,\text{GHz}$, due to a transmission notch of more than 20 dB that extensively exceeds the criterion's requirements, a bandwidth of $\Delta f_{\text{notch}} \approx 1.0\,\text{GHz}$ satisfies the demand for a taper offering submillimeter accuracy. This fact confirms the worst case estimation given by the proposed design criterion according to Sect. 3.3. Finally, the application of such a metallic obstacle causes no major impairments concerning the input matching behavior of the first port. Although not having been an integral part of our investigation, a value of $\left|S_{1(\text{H}_{11}),1(\text{H}_{11})}\right| < -10\,\text{dB}$ is reached over the frequency range of operation. Further effort on this quantity could be spent in the design process of a corresponding prototype taper based on this promising concept.

5 Conclusions

In this paper, compact mode-matched excitation structures for the application in FMCW radar distance measurements in still pipes have been fundamentally investigated. These structures are tapers that function as waveguide transitions between circular waveguides of different diameters. By establishing a still pipe simulator, incorporating all effects of multimode propagation, it was shown that intermodal dispersion effects, caused by spurious mode excitation, dominates the measurement uncertainties, if common signal processing algorithms are deployed. This leads to a great demand of a design criterion, that appropriately accounts for the spurious mode attenuation as well as for the suppression bandwidth to accomplish certain measurement specifications, e.g. for augmenting the accuracy level to the submillimeter domain. Finally, a novel subreflector-based taper concept was introduced, exhibiting promising mode suppression levels. By verifying the corresponding distance error, it was clarified that this concept meets the requirements for FMCW high-precision level detection conducted in large overmoded circular waveguides.

References

Barrow, W.: Transmission of electromagnetic waves in hollow tubes of metal, Proceedings of the IEEE, 72, 1064–1076, 1984.

Brumbi, D.: Measuring process and storage tank level with radar technology, Radar Conference, 1995., Record of the IEEE 1995 International, pp. 256–260, doi:10.1109/RADAR.1995.522555, 1995.

Brumbi, D.: Low power FMCW radar system for level gaging, Microwave Symposium Digest., 2000 IEEE MTT-S International, 3, 1559–1562 vol.3, doi:10.1109/MWSYM.2000.862273, 2000.

Fernandez Casares, S. and Balle, S. M.-V. P.: Mode beating and spontaneous emission noise effects in a variable-waveguide model for the dynamics of gain-guided semiconductor laser arrays, IEEE J. Quantum Electronics, 30, 2449–2457, doi:10.1109/3.333695, 1994.

Hartog, A.: Influence of waveguide effects on pulse-delay measurements of material dispersion in optical fibres, Electronics Lett., 15, 632–634, doi:10.1049/el:19790450, 1979.

Katsenelenbaum, B. Z. and Mercader, L. P. M. S. M. T. M.: Theory of Nonuniform Waveguides: The Cross-Section Method, vol. 44, ser. IEE Electromagn. Waves. London, U.K., IEE Press, 1998.

Kielb, J. A. and Pulkrabek, M.: Application of a 25 GHz FMCW radar for industrial control and process level measurement, Microwave Symposium Digest, 1999 IEEE MTT-S International, 1, 281–284, doi:10.1109/MWSYM.1999.779475, 1999.

Le Huerou, J.-Y. and Gindre, M. A. A. U. W. W. M.: Compressibility of nano inclusions in complex fluids by ultrasound velocity measurements, IEEE Transactions on Ultrasonics, Ferroelectrics and Frequency Control, 50, 1595–1600, doi:10.1109/TUFFC.2003.1251143, 2003.

Musch, T.: A high precision 24-GHz FMCW radar based on a fractional-N ramp-PLL, Instrumentation and Measurement, IEEE Trans., 52(2), 324–327, doi:10.1109/TIM.2003.810046, April 2003.

Narasimhan, M. S. and Balasubramanya, K.: Transmission Characteristics of Spherical TE and TM Modes in Conical Waveguides (Short Papers), IEEE Trans. Microwave Theory and Techniques, 22, 965–970, 1974.

Parker, S.: Diverse uses for level radar, InTech, ISA International Society for Measurement and Control, May 2002.

Pohl, N. and Gerding, M. W. B. M. T. H. J. S. B.: High Precision Radar Distance Measurements in Overmoded Circular Waveguides, IEEE Trans. Microwave Theory and Techniques, 55, 1374–1381, doi:10.1109/TMTT.2007.896784, 2007.

Rusch, W.: Scattering from a hyperboloidal reflector in a cassegrainian feed system, IEEE Trans. Antennas and Propagation, 11, 414–421, 1963.

Sai, Bin and Kastelein, B.: Advanced High Precision Radar Gauge for Industrial Applications, International Conference on Radar, 2006. CIE '06., pp. 1–4, doi:10.1109/ICR.2006.343173, 2006.

Shum, M. L. P.: Effects of intermodal dispersion on short pulse propagation in an active nonlinear two-core fiber coupler, Photonics Technology Lett., IEEE, 16, 1080–1082, doi:10.1109/LPT.2004.824994, 2004.

Stolle, R. and Heuermann, H. S. B.: Novel algorithms for FMCW range finding with microwaves, Microwave Systems Conference, 1995. Conference Proceedings., IEEE NTC '95, pp. 129–132, doi:10.1109/NTCMWS.1995.522875, 1995.

Tang, C.: Mode Conversion in Tapered Waveguides At and Near Cutoff, IEEE Trans. Microwave Theory and Techniques, 14, 233–239, 1966.

Weiss, M.: Low-cost, low-power nanosecond pulse radar for industrial applications with mm accuracy, 2001 International Symposium on Electron Devices for Microwave and Optoelectronic Applications, pp. 199–204, doi:10.1109/EDMO.2001.974307, 2001.

Weiss, M. and Knochel, R.: A Highly Accurate Multi-Target Microwave Ranging System for Measuring Liquid Levels in Tanks, 27th European Microwave Conference, 1997, 2, 1103–1112, doi:10.1109/EUMA.1997.337945, 1997.